Published in final edited form as:
Comput Theor Chem. 2012 February 1; 981: 73–85. doi:10.1016/j.comptc.2011.11.049.

Revealing substituent effects on the electronic structure and planarity of Ni-porphyrins

Jenna Barbee and **Aleksey E. Kuznetsov***
Department of Chemistry, Duke University, Durham, NC 27708, USA

Abstract

Using density functional theory, we have studied the effects on structural and electronic consequences (including HOMO-LUMO energy gaps, vertical ionization potentials (IP_v), and vertical electron affinities (EA_v)) of the following two factors: (a) *meso*- and β-substituents acting as inductive donors (CH_3), inductive acceptors that are electron-donating through resonance (Br), inductive electron acceptors (CF_3), and resonance enabled acceptors (NO_2); and (b) *complete replacement* of pyrrole nitrogens with P-atoms. The principal results of the study are: (1) For the bare Ni-porphyrin, the solvents were found not to affect the HOMO–LUMO gaps but to change the IP_v and EA_v noticeably. (2) In the series $CH_3 \rightarrow Br \rightarrow CF_3 \rightarrow NO_2$ the HOMO-LUMO energy gaps, IP_v, and EA_v increase for both *meso*- and β-substituents. The ruffling distortion of the porphyrin core is retained, and becomes stronger for the two acceptor groups. In general, effects of *meso*-substituents on the ruffling distortion of the porphyrin core is more pronounced. (3) Most significantly, complete replacement of pyrrole nitrogens in the NiP with phosphorus atoms produces the species, $NiP(P)_4$, with the structural and electronic features drastically different from the original NiP. This implies that $NiP(P)_4$ can possess interesting and unusual novel properties, including aromaticity and reactivity, leading to its various beneficial potential applications. Furthermore, $NiP(P)_4$ high stability both in the gas phase and different solvents was shown, implying the feasibility of its synthesis.

1. Introduction

Metalloporphyrins and their derivatives are of great interest because of their role in biology as enzyme cofactors [1–8] and also due to their numerous technological applications [9–23]. Pronounced features of porphyrins which largely define their properties and functions, along with aromaticity [24–28], is their conformational flexibility [1–5,29–45]. Porphyrin nonplanarity is a rather general phenomenon [1–5,29–45,46–48]. Its most signifi-cant consequence is the decrease of $C_\alpha—C_m—C_\alpha$ bond angles (see Fig. 1a for the porphyrin core labeling scheme). The distance between the center of the porphyrin core (metal ion) and the pyrrole nitrogens, corresponding to the minimization of core radial strain, was found to be close to 2.01 Å [46–48].

The degree of nonplanarity of metalloporphyrins primarily depends on such factors as the size of the central metal, the substituent size, shape, and orientation, pyrrole nitrogen(s) substitution by other elements, etc. [29–50] (see Fig. 2). Ni^{II}-porphyrins show a rich conformational behavior: a $(d_{z2})^2$ electronic configuration and small ionic radius, 0.69 Å [51], of Ni^{II} favor relatively short equilibrium Ni—N bond distances. This results in nonplanar ruffled Ni-porphyrin conformations [30,48] (see Fig. 1b) in which individual pyrrole rings are twisted about the Ni—N axes and significant alternating displacements of

*Corresponding author. Tel.: +1 9196601634; fax: +1 9196601605. ak189@duke.edu (A.E. Kuznetsov).

the C_m sites above and below the mean molecular plane take place [31]. Over the past four decades, theoretical studies of effects of various factors, such as substituents, central metal type, and annulation, etc. on structures and properties of Ni-porphyrins and their derivatives have been numerous [28,32–33,52–80]. Nonetheless, to the best of our knowledge, so far no *systematic* theoretical studies of the effects of important factors which could result in porphyrin moiety distortions and changes in structural and electronic properties of Ni-porphyrins (see Fig. 2) have been performed. It is of high interest to clarify systematic effects of the following two factors: (a) relatively *simple* substituent groups of "classical" organic chemistry types: inductive donors (exemplified by aklyls), inductive acceptors that are electron-donating through resonance (for instance, halogens), inductive electron acceptors (fluorinated alkyls), and resonance enabled acceptors (such as nitro groups), and (b) *complete replacement of pyrrole nitrogens with heavier congener*(*phosphorus*) on geometries and electronic features (including HOMO–LUMO energy gaps, vertical ionization potentials, and electron affinities) of Ni-porphyrins.

Effects of the central metal on structural properties of unsubstituted metalloporphyrins (MPs), including Ni-porphyrins, were studied previously by Kozlowski and co-workers [53–58]. In the 2009 DFT study of chemical bonding and aromaticity of a series of MPs [28] the D_{4h} structure was shown to be a global minimum for NiP. Liao and Scheiner performed DFT studies of electronic structure and bonding in MPs and MTPPs [59] and in MPs, metalloporphyrazines (MPz), and metallophthalocyanines (MPc) [60] including Ni-species. Electronic structures of series of neutral, cationic, and anionic MPs, including NiP, were studied using restricted Hartree-Fock (RHF) and Singles and Doubles Configuration Interaction (SDCI) methods [61]. In the earlier work [62] neutral and anionic species of the same MPs were studied using the RHF approach. Five- and six-coordinate Ni^{II}- and V=O-porphyrins in petroleum were explored [63], with Ni- and V=O-octaethylporphyrins used as model systems, with or without NO_2-groups in *meso*-positions. Systematic DFT study of the structures, properties and reactivity of $(pyridine)_n$-MP complexes (M = Mg, Ca, Cr, Mn, Co, Ni, Cu, Zn, Ru, and Cd; n = 0, 1, or 2) was performed by Feng and co-workers [64,65]. Investigations of optical properties of MPs (M = Mg, Ni, Zn), MTPPs (M = Mg, Ni, Zn) [66], NiOMTP (OMTP = 2,3,7,8,12, 13,17,18-octakismethylthioporphyrin) [67], and NiOEP [66,68] were carried out using TDDFT [66,67] and ZINDO approaches [68]. Electronic effects of *meso*-tetraaza substitution and tetrabenzo annulation on the structures and optical properties in the series NiP, NiPz, NiTBP (Ni-tetrabenzoporphyrin), and NiPc were studied [69]. For the series of MPs (M = H_2, Zn, Mg, Ni, Fe^{II}, P^{V}, Si^{IV}; for M = Mg and Ni octa-Br-substituted porphyrins studied as well) Ghosh and Ryeng confirmed [70] the previous finding that ruffling does not engender significant red shifts in the Q- and B-band energies of simple (metallo)porphyrins [71] and extended this finding to the saddling case. Kozlowski and co-workers performed theoretical analysis of singlet and triplet excited states of NiP, NiOEP, and NiTPP [72], and Zamyatin and co-workers [73] performed combined theoretical and kinetic spectrometric investigation of Ni^{II}-tetraphenyl tetrabenzoporphyrin. Guo and co-workers [74] studied ligand substitution effect on electronic structure and optical properties of a variety of planar conjugated Ni-centered macrocycles. Also, it is worth mentioning studies by Shelnutt and co-workers on various Ni-porphyrins using the molecular mechanics (MM) and ab *initio* approaches [32,33,75–80].

Effects of replacement of pyrrole nitrogens by heavier congeners (P) were studied both on bare and metallated porphyrins and their derivatives. In 2003 Delaere and Nguyen [81] reported the DFT study of the structural and optical properties of the P-porphyrins with one or two P-atoms. Matano, Nakabuchi, Imahori and co-workers [82–89] reported syntheses and characterization of various phosphaporphyrins [82–89], phosphacalixphyrins [83,85,89,90] and phosphacalixpyrroles [85] with only one pyrrole nitrogen replaced by P-atom. Several metal complexes were studied as well [82,87,90]. Along with experimental

characterizations, DFT studies were performed on free bases [82,84–90] and metal complexes [82] investigated.

Many of the theoretical studies reviewed above consider either effects of quite complex substituting groups or effects of several factors together, which could make it difficult to separate concomitant changes in Ni-porphyrin structural and electronic properties. In this paper, we first address the *separate* effects on structural and electronic properties (including HOMO–LUMO energy gaps, vertical ionization potentials (IP_v), and electron affinities (EA_v)) of the *meso*- and β-substituting groups acting as inductive donors (CH_3), inductive acceptors that are electron-donating through resonance (Br), inductive electron acceptors (CF_3), and resonance enabled acceptors (NO_2). Next, we consider changes which the *complete replacement of pyrrole nitrogens with phosphorus* would cause in the geometry and electronic properties of the Ni-porphyrin species.

2. Computational details

All calculations described here were performed using the Gaussian03 package [91]. Geometries of all species under investigation were optimized starting with symmetric structures, and the structures obtained were checked to be real global minima by vibrational frequencies computation. If imaginary frequencies were found, further optimizations along those frequencies without any symmetry constraint were performed. For all species under investigation, we studied both singlet and triplet spin states and performed thorough global minimum search. Calculations were performed using the split-valence 6-31G* basis set [92–96] and the hybrid B3LYP functional [97]. This approach was earlier shown to give geometries in a good agreement with experiments (see, e.g., [53]), and is subsequently referred to as B3LYP/6-31G*. The solvent effects were estimated at the B3LYP/6-31G* level of theory using the self-consistent reaction field IEF-PCM method [98] (UA0 model) with water, benzene, and acetonitrile as solvents (dielectric constants ε = 78.39, 2.247, and 36.64, respectively). Below, we discuss gas phase energetics ΔE (without zero point correction) calculated at the B3LYP/6-31* level of theory. Plots of molecular orbitals and pictures of structures were obtained using the Molekel 5.4.0.8 visualization software [99].

3. Results and discussion

3.1. Bare Ni(II)-porphyrin species

The singlet D_{2d} structure of Ni-porphyrin (NiP) was found to be more stable than the D_{4h} species both in the gas phase and in three solvents, by just 0.2 (2.4, 0.1, 0.2 in water, benzene, and acetonitrile, respectively) kcal/mol at the B3LYP/6-31G* level of theory, in good agreement with the results of Kozlowski and co-workers [53]. Both in the gas phase and in solution (independently of the solvent used in the calculations), the D_{4h} structure was found to have small imaginary frequency, *ca.* 30 cm^{-1}, responsible for ruffling distortions of the porphyrin core. The triplet state of NiP (in C_1 symmetry) was found to be 8.0 (6.1, 7.8, 6.6) kcal/mol above the singlet D_{2d} structure. Structural parameters of the singlet D_{2d} and triplet C_1 structures calculated in the gas phase along with experimental data are given in Table 1, and atom labeling scheme can be seen in Fig. 3a. Table 2 summarizes Mulliken analysis results for the singlet and triplet NiP species. (We provide the results of calculations with solvent effects included in supporting information, Section 1; for the full set of calculated structural parameters of the singlet D_{2d} and triplet C_1 structures, see Table S1, for the Mulliken analysis results, see Table S2.)

Analysis of the data above shows that: (i) in the gas phase, the global minimum singlet structure is slightly less flattened compared with the solution phase (see supporting information for the calculated structural parameters); (ii) the low-lying triplet structure,

which is essentially of the C_2 symmetry, is much less ruffled compared to the global minimum singlet and remains essentially flat both in the gas phase and in the solvent phase (see supporting information); (iii) in the triplet structure, the Ni-N distances are noticeably elongated compared to the global minimum structure, by 0.08 Å in the gas phase, which facilitates flattening of the triplet structure; (iv) calculated geometry parameters are in good agreement with experimental data; (vi) in the triplet structure, the Ni center bears a charge increased by about 0.13-0.16e compared to the global minimum singlet and bears most part of the total spin density, more than 1.7e (α-spin), which is ferromagnetically coupled with spins on pyrrole nitrogens (about 0.05e of α–spin density each).

Fig. 3b shows two HOMOs and two LUMOs of the global minimum D_{2d} singlet NiP structure. Both HOMO/HOMO − 1 and LUMO/LUMO' have dominating contributions from the porphyrin ring and small contributions from the Ni d-orbitals. Inclusion of the solvent effects does not influence significantly the orbital energies: the HOMO-LUMO energy gap was calculated to be 3.13 eV in the gas phase and 3.15, 3.13, and 3.15 eV in water, benzene, and acetonitrile, respectively. These numbers are quite in disagreement with the theoretical gas phase results of Liao and Scheiner, 2.10 eV [60], and with the results of Ryeng and Ghosh, 2.37–2.4 eV [70], and also with the experimental value 2.10–2.30 eV, reported from the electrochemical measurements for series of octaethyl- and tetraphenylporphyrins [101], but they agree very well with the results reported for the NiP CS_2 solution, 3.11 eV for the NiP B band (we understand that the calculated HOMO–LUMO energy gap should be compared with the experimental spectral data with high caution) [100]. Discrepancies in the results could be explained by the difference of the approaches used. The IP_v and EA_v values for the singlet D_{2d} species were calculated to be 6.59 and 0.74 eV, respectively. These numbers are in reasonable agreement with the theoretical results of Liao and Scheiner, 7.01 and 1.31 eV, respectively [60]. Again, differences could be explained by different approaches used. Solvent effects were found to be quite significant: IP_v ($H_2O/C_6H_6/CH_3CN$) = 5.43/5.06/5.18 eV, EA_v ($H_2O/C_6H_6/CH_3CN$) = 2.35/1.58/2.30 eV. To our surprise, we were unable to find any experimental data for IP_v and EA_v of the NiP species. Interestingly, our calculated gas phase IP_v value, 6.59 eV, appears to be relatively close to the gas phase value, 6.44 eV, obtained by photoelectron spectroscopy for Ni-tetraphenylporphyrin [102].

3.2. Meso-substituted Ni(II)-porphyrin species

3.2.1. Structural features and Mulliken analysis results

3.2.1.1. CH_3-substituents: The global minimum singlet C_2 NiP(*meso*-CH_3)$_4$ species is shown in Fig. 4a, and its calculated gas phase structural parameters and Mulliken charges are provided in Tables 3 and 4, respectively. The lowest-lying triplet (in C_1 symmetry, see Table S6 in supporting information) was calculated to be 13.8 kcal/mol higher in the gas phase. Comparison between the D_{2d} NiP and C_2 NiP(*meso*-CH_3)$_4$ shows the following changes in geometry and electronic structure (Tables 1-5): (i) in NiP(*meso*-CH_3)$_4$ the Ni—N bond distance is shortened by 0.03 Å and C_α—C_m bond distance is elongated by 0.02 Å, and the whole NiP(meso-CH_3)$_4$ molecule becomes noticeably more ruffled, the C_m–Ni–C_m' angle being decreased by 11.10°; (ii) Mulliken charges on Ni, N's, C_a, and Cb in NiP(*meso*-CH_3)$_4$ change by −0.03, 0.0, −0.06, and 0.0e, respectively, whereas charges on C_m change from −0.28 to 0.05e; (iii) the inductive electron-donating effect of the CH_3-groups causes *destabilization* of the HOMO by 0.36 eV and of the LUMO by 0.11 eV, which leads to the *decrease* of ΔE (HOMO–LUMO) by 0.25, IP_v by 0.48, and EA_v by 0.06 eV, respectively. The NiP(*meso*-tBu)$_4$ species, calculated for comparison purposes, has shorter Ni—N bond distances, 1.89 Å vs. 1.91 Å in the NiP(*meso*-CH_3)$_4$ molecule, and longer C_α—C_m bond distances, 1.42 Å vs. 1.40 Å in NiP(*meso*-CH_3)$_4$. The whole NiP(*meso*-tBu)$_4$ structure is

even more ruffled then the NiP(*meso*-CH_3)$_4$ species: the C_m–Ni–C_m' angle is 140.8° compared to 156.4° in NiP(*meso*-CH_3)$_4$. However, Mulliken charges on C_m again changed significantly, from −0.28 (bare NiP) to just 0.01e, very similar to NiP(*meso*-CH_3)$_4$ case. Thus, the stronger inductive electron-donating effect of a *meso*-substituent is, the stronger binding interactions between Ni and N's become and thus the shorter Ni—N distances are, which results in increased ruffling of the whole molecule. Also, the stronger inductive electron-donating effect of the *meso*-substituent causes larger weakening of the C_α—C_m bonds. ΔE(HOMO–LUMO) of the NiP(*meso*-tBu)$_4$ structure is further decreased to 2.67 eV compared to 2.88 eV of NiP(*meso*-CH_3)$_4$ (see Table 5).

3.2.1.2. Br-substituents: The S_4 symmetry of the global minimum NiP(*meso*-Br)$_4$ species (Fig. 5a) makes it similar to the tetragonal ruffled conformer of NiOEP (which, however, was found to be not a global minimum but the second low-lying conformer) [52]. A low-lying triplet in S_4 symmetry was found to be 11.4 kcal/mol higher (see Table S7). Comparison between the bare NiP and NiP (*meso*-Br)$_4$ shows that (see Tables 1-5): (i) in NiP(*meso*-Br)$_4$ the Ni—N distance is shortened by 0.02 Å and C_α—C_m bond distance is elongated by 0.01 Å, and again the whole NiP(*meso*-Br)$_4$ molecule is more distorted compared to the parent NiP species, with the C_m–Ni–C_m' angle decreased by 10.10°; (ii) Mulliken charges on Ni-, N-, C_α-, and C_β-atoms in NiP(*meso*-Br)$_4$ are changed by 0.01, −0.01, −0.03, and 0.01e, respectively, whereas charges on C_m decrease by 0.22e, from −0.28 to −0.06e; (iii) the resonance electron-donating effect of the Br-groups causes *stabilization* of the HOMO by 0.37 eV and of the LUMO by 0.65 eV, which leads to the more pronounced decrease of the HOMO—LUMO energy gap compared to the CH_3-substitutents, by 0.29 eV. Consequently, in contrast with the previous situation, both IP_v and EA_v are *increased,* by 0.18 and 0.75 eV, respectively. Comparison with the S_4 NiP(*meso*-SH)$_4$ species shows that it has very similar geometry, with Ni—N bond distances being 1.91 Å vs. 1.92 Å in NiP(*meso*-Br)$_4$, and the C_m–Ni–C_m' angle 157.7° compared to 157.4° in NiP(*meso*-Br)$_4$. However, Mulliken charges on C_m in the NiP(*meso*-SH)$_4$ species are significantly larger, −0.25e, very close to the −0.28e value in the bare NiP. The HOMO—LUMO gap of the NiP(*meso*-SH)$_4$ species is 2.71 eV compared to 2.84 eVof theNiP(*meso*-Br)$_4$ compound (Table 5). Thus, using *meso*-substituents acting as inductive acceptors/electron donors through resonance with different electronegativities (Br, 2.96; S, 2.58) [51] did not affect geometries significantly, but caused pronounced changes in electronic properties, telling about the simple way of tuning the electronic properties of *meso*-substituted NiPs.

3.2.1.3. CF_3-substituents: For the CF_3-*meso*-substituted species, the singlet C_2 structure (Fig. 6a) was found to be a global minimum. Also, we found five essentially degenerate triplets, all located around 39 kcal/mol higher in energy (see Table S8). Compared to the bare NiP species, in the NiP(*meso*-CF_3)$_4$ species the Ni—N bond distances are shortened by 0.05 Å and the C_α—C_m bond distances are elongated by 0.02 Å, and the C_m–Ni–C_m' angles are decreased by 16.9°; the Mulliken charges on Ni, pyrrole N's, C_α, and C_β in NiP(*meso*-CF_3)$_4$ change by −0.01, −0.01, −0.05, and 0.01e, respectively, whereas charges on C_m change by 0.14e; the carbons of the CF_3-groups bear large positive charge, 0.82e (Table 5); the inductive electron-withdrawing effect of the CF_3-groups *stabilizes* HOMO by 0.77 eV and LUMO by 1.06 eV, which leads to the *decrease* of ΔE(HOMO—LUMO) by 0.29 and causes drastic *increases* of IP_v and EA_v, by 0.69 eV and 1.08 eV, respectively (Table 5), in agreement with the results of Liao and Scheiner [60].

3.2.1.4 NO_2-substituents: For the NO_2-*meso*-substituted Ni-porphy-rin, we found the singlet S_4 structure (Fig. 7a) to be a global minimum. The lowest-lying triplet having C_1

symmetry was calculated to be 8.1 kcal/mol higher, and the triplet structure with S_4 symmetry located 9.6 kcal/mol higher was found as well (see Table S9).Apparently, the singlet S_4 structure with NO_2-groups rotated relative the porphyrin plane is preferred over the flat D_{2h} structure to minimize steric repulsions between oxygens of the NO_2-groups and β-hydrogens. Compared to the bare Ni-porphyrin, in S_4 NiP(*meso*-NO_2)$_4$ the Ni—N bond distances are shortened by 0.02 Å and the C_α—C_m bond distances are elongated by mere 0.01 Å, and the C_m–Ni–C_m' angles are decreased by 9.8°; the Mulliken charges on Ni, pyrrole nitrogens, C_α, and C_β in NiP(*meso*-NO_2)$_4$ change by 0.02, −0.03, 0.0/0.01, and 0.02/0.03e, respectively, whereas charges on C_m are increased by 0.43e; the nitrogens and oxygens of the NO_2-groups bear considerable charges, 0.33 and −0.36/−037e, respectively (Table 4); the resonance electron-withdrawing effect of the NO_2-groups also significantly *stabilizes* HOMO and LUMO, by 1.38 and 1.81 eV, respectively (Table 5). This decreases the ΔE(HOMO—LUMO) by 0.43 eV and causes even more pronounced *increase* of IP_v and EA_v, by 1.76 eV and 1.88 eV, respectively (see Table 5).

3.2.2. Molecular orbitals comparison with the bare NiP species—Generally, one of the considered HOMOs of the *meso*-substituted NiP species looks very similar to the D_{2d} NiP MO of the same topology, and another considered HOMO of the *meso*-substituted NiP species usually has more pronounced contributions from Ni compared with the bare NiP (and thus stronger bonding Ni—N interactions), with some contributions from the *meso*-substituents as well (cf. Figs. 3b and 4b, 5b, 6b, 7b). It is the HOMO in NiP(*meso*-CH_3)$_4$ and in NiP(*meso*-Br)$_4$ (where noticeable contributions from bromines are in anti-phase with the (C_α—C_m—C_α) contributions, see Fig. 5b) and the HOMO − 1 in NiP(*meso*-CF_3)$_4$ and in NiP(*meso*-CF_3)$_4$ (see Figs. 6b and 7b). In two last species, the electron density of the HOMO −1 is noticeably polarized towards the substituents. Both LUMO and LUMO + 1 of the NiP(*meso*-CH_3)$_4$ species are essentially degenerate MOs, with energies −0.07227 and −0.07226 a.u., respectively, and could be considered as a mixture of degenerate *e*-type LUMO/LUMO' of the D_{2d} NiP (see Figs. 3b and 4b) with some contributions from the methyl groups. LUMO and LUMO' of NiP(*meso*-Br)$_4$ are degenerate *e*-type MOs and could be considered as slightly distorted degenerate *e*-type LUMO/LUMO' of the D_{2d} NiP (see Figs. 3b and 5b) with some contributions from the bromines. LUMO and LUMO + 1 of NiP(*meso*-CF_3)$_4$ could be considered as slightly distorted degenerate *e*-type LUMO/LUMO' of the D_{2d} NiP (see Figs. 3b and 6b) with pronounced shift of the electron density towards the substituents. Both LUMO/LUMO' of NiP(*meso*-NO_2)$_4$ could be considered as noticeably distorted degenerate *e*-type LUMO/LUMO' of the D_{2d} NiP (see Figs. 3b and 7b) with pronounced shift of the electron density towards the substituents.

3.3. β-Substituted Ni(II)-porphyrin species

3.3.1. Structural features and Mulliken analysis results

3.3.1.1. CH_3-substituents: The global minimum singlet C_1 NiP(β-CH_3)$_8$ species is shown in Fig. 8a, and its calculated gas phase struc-tural parameters and Mulliken charges are given in Tables 6 and 7, respectively. The low-lying triplet in C_1 symmetry was calculated to be 10.7 kcal/mol above the global minimum, and another lower-lying triplet in C_{2v} symmetry (^{3}B1 state) was found to be 8.3 kcal/mol higher (see Table S10 in supporting information). The following features of the NiP(β-CH_3)$_8$ geometrical and electronic structures can be highlighted (see Tables 1, 2, 6 and 7): (i) only the C_α—C_β and C_β—C_β bond distances in NiP(β-CH_3)$_8$ are changed noticeably, both being elongated by 0.01 Å; the whole NiP(β-CH_3)$_8$ molecule remains almost undistorted compared to the original D_{2d} singlet NiP structure, the C_m–Ni–C_m' angles being *increased* by mere 0.5/0.6°; (ii) Mulliken charges on Ni, pyrrole nitrogens, C_α, and C_m in NiP(β-CH_3)$_8$ change negligibly by −0.02, −0.03, −0.03, and −0.01e, respectively, whereas charges on C_β change from −0.18 to 0.07e;

(iii) the inductive electron-donating effect of the CH_3-groups causes some destabilization of HOMO and LUMO, by 0.48 and 0.32 eV, which is more pronounced than in the case of the *meso*-substituted species (see Table 5). This leads to the decrease of ΔE(HOMO—LUMO)by 0.16, IP_v by 0.64, and EA_v by 0.23 eV, respectively (see Table 8).

3.3.1.2. Br-substituents: The global minimum singlet NiP(β-Br)$_8$ species (Fig. 9a) was found to have C_1 symmetry. The lowest-lying triplet (C_1) was calculated to be 6.1 kcal/mol higher (Table S11 in supporting information). Interestingly, in the β-Br-substituted species no bond distances are changed noticeably compared to the original D_{2d} NiP structure (see Tables 1 and 6), and again the whole NiP(β-Br)$_8$ molecule remains almost undistorted compared to the original D_{2d} singlet NiP structure, the C_m–Ni–C_m' angles being *increased* by mere 0.6°. Mulliken charges on Ni-, N-, C_α-, and C_m-atoms change by 0.03, −0.03, 0.0, and 0.02e, respectively, whereas charges on C_β change from −0.18 to −0.26e. Finally, the inductive electron-donating effect of the bromines in the β-positions *stabilizes* both HOMO and LUMO of NiP(β-Br)$_8$, by 0.75 and 0.90 eV, which is again more pronounced than in the case of the *meso*-substituted species (see Table 5). This leads to the decrease of ΔE(HOMO—LUMO) by 0.16, and increase of IP_v by 0.49 and EA_v by 1.10 eV, respectively (see Table 8).

3.3.1.3. CF_3-substituents: We found the global minimum structure to be a singlet species with C_1 symmetry (Fig. 10a). The lowest-lying triplet (with C_1 symmetry) is located 11.1 kcal/mol above the global minimum (see Table S12). In sharp contrast with the β-CH_3- and β-Br-substituted compounds, in the β-CF_3-substituted NiP noticeable changes in geometry are observed compared to the original NiP (see Tables 1 and 6): the Ni—N and N—C_α bond distances are shortened by 0.03 and 0.01 Å, respectively, the C_α—C_β, C_β—C_β and C_α—C_m bond distances are elongated by 0.01, 0.01 and 0.01 Å, respectively, and the whole NiP(β-CF_3)$_8$ molecule becomes quite significantly distorted (ruffled) compared to the original D_{2d} NiP structure: the C_m–Ni–C_m' angles are *decreased* by 11.2°. Mulliken charges on Ni-, N-, C_α-, and C_m-atoms are changed by 0.03, −0.03, −0.02, and 0.02e, respectively, whereas charges on C_β are changed by 0.06e. Significant charges are located on substituent atoms: 0.85e on carbons and −0.25/−0.26/−0.27e on fluorines. Finally, the inductive electron-withdrawing effect of the CF_3-groups in the β-positions *stabilizes* both HOMO and LUMO of NiP(β-CF_3)$_8$, by 1.48 and 1.69 eV, respectively, again more pronounced than in the case of the *meso*-substituted counterpart (see Table 5). This stabilization leads to the decrease of ΔE(HOMO–LUMO) by 0.21, and drastic *increase* of IP_v, by 1.35, and EA_v, by 1.81 eV (Table 8), respec-tively, in agreement with the results of Liao and Scheiner [60].

3.3.1.4. NO_2-substituents: The global minimum structure is a singlet species with C_1 symmetry (Fig. 11a), and the low-lying triplet (with C_1 symmetry) is located 33.5 kcal/mol above the global minimum (Table S13 in supporting information). Apparently, NO_2-groups in β-positions should undergo strong steric repulsions and thus are rotated relative to the porphyrin plane. Again, in sharp contrast with the above cases of β-CH_3- and β-Br-substituted compounds, in the β-NO_2-substituted Ni-porphyrin noticeable changes in geometry are observed compared to the original Ni-porphyrin (see Tables 1 and 6): the Ni—N bond distances are shortened by 0.02 Å, respectively, and the whole NiP(β-NO_2)$_8$ species becomes more distorted (ruffled) compared to the original NiP structure: the C_m–Ni–C_m' angles are *decreased* by 8.8°. Mulliken charges on Ni-, N-, C_α-, and C_m-atoms are changed by 0.06, −0.05, 0.01, and 0.05/0.06e, respectively, whereas charges on C_β are changed by 0.06e. Substituent groups bear the charges of 0.17e and −0.35/−0.36e on nitrogens and oxygens, respectively. Finally, the resonance electron-with drawing effect of the NO_2-groups in the β-positions *stabilizes* both HOMO and LUMO of NiP(β-NO_2)$_8$ even more significantly than other substituents in the p-positions, by 2.50 and 2.97 eV, respectively,

which is again more pronounced than in the case of the *meso*-substituted species (see Table 5). This stabilization leads to the significant decrease of ΔE(HOMO–LUMO) by 0.47, and strong *increase* of IP_v, by 2.31, and EA_v, by 3.13 eV, respectively (see Table 8).

3.3.2. Molecular orbitals comparison with the bare NiP species—Again, as in the *meso*-substituted NiP species case, one of the considered HOMOs of the β-substituted NiP species looks very similar to the D_{2d} NiP MO of the same topology, and another considered HOMO of the β-substituted NiP species usually has more pronounced contributions from Ni compared with the bare NiP (and thus stronger bonding Ni—N interactions) (cf. Figs. 3b and 8b, 9b, 10b, 11b). It is the HOMO − 1 in NiP(β-CH_3)$_8$ and NiP(β-Br)$_8$, and the HOMO in NiP(β-CF_3)$_8$ and NiP(β-NO_2)$_8$ (see Figs. 10b and 11b), similar to the *meso*-substituted NiP species case. Both LUMO and LUMO + 1 of all the four β-substituted NiP species are essentially degenerate and could be considered as counterparts of degenerate *e*-type LUMO/LUMO' of the D_{2d} NiP (cf. Fig. 3b), with some contributions from substituents for Br-, CF_3-, and NO_2-groups.

4. Heavy atom effect: Ni(II)-porphyrin with pyrrole nitrogens completely replaced by phosphorus

We also studied the effect of the *complete replacement of pyrrole nitrogens* in the NiP by heavier congener, namely, by the phosphorus atoms, and the resulting structure and its two HOMOs and LUMOs are shown in Fig. 12a and b, respectively. The most unusual and intriguing result of this substitution is strong deformation of the resulting NiP(P)$_4$, which attains bowl-like shape, with the C_m–Ni–C_m' angles being about 21° smaller than in the parent NiP (see Tables 1 and 9). This is in line with the results obtained previously in theoretical [81,82,84–90] and experimental [82–90] studies of phosphaporphyrins [82–89], phosphacalixphyrins [83,85,89,90] and phosphacalixpyrroles [85] where deviations from planarity were found as well, although in our case they are much more pronounced. The Ni—P and P—$C_α$ bond distances are considerably longer than the Ni—N and N—$C_α$ bond distances, by ca. 0.2 and 0.4 Å in the gas phase, respectively. Also, the $C_β$—$C_β$ and $C_α$—C_m bond distances in the NiP(P)$_4$ are longer than in the NiP, by ca. 0.2 and 0.2 Å in the gas phase, respectively. The very important geometrical parameter to be considered here is the $C_α$—P—$C_α$ angle, which is ca. 11° larger than the corresponding $C_α$—N—$C_α$ angle in the parent NiP: this significant difference is due to the smaller hybridization (larger *s*-character) of the P-atom valence orbitals, and it along with long Ni—P and P—$C_α$ bond distances explains the drastic distortion of the P—Ni-porphyrin, both in the gas phase and in solvents. Comparing the Mulliken analysis results from the Tables 2 and 10 shows another noticeable differences between the NiP(P)$_4$ and original Ni-porphyrin, namely, *negative* charges on the Ni and $C_α$-centers (and *positive* charge on the P-atoms) in the former compared to the *positive* charge on the Ni and $C_α$-centers (and *negative* charge on the N-atoms) in the latter. This might result in drastic changes of the reactivity pattern of the NiP(P)$_4$ compound and its potential novel applications, e.g., in catalysis. The NiP(P)$_4$ HOMO/LUMO energies (a.u.) were calculated to be −0.19496/−0.10062 vs. −0.19123/−0.07632 for NiP, thus, the noticeable LUMO *stabilization* is observed in NiP(P)$_4$. The calculated gas phase HOMO–LUMO energy gap of NiP(P)$_4$ is 2.57 eV, IP_v is 6.51 eV, and EA_v is 1.46, compared to 3.13, 6.58, and 0.74 eV for NiP. We also found the reaction

$$\mathrm{NiP(P)_4} \rightarrow [\mathrm{P-porphyrin}]^{2-} + \mathrm{Ni}^{2+}$$

to be *endothermic* by 728.9 kcal/mol in the gas phase and by 124.7, 396.6, and 134.2 kcal/mol in H_2O, C_6H_6, and CH_3CN, respectively. These data imply that the $NiP(P)_4$ species should be stable in solution and could be successfully synthesized.

The completely P-substituted Ni-porphyrin species can be considered as derivatives of tetraphosphole compound. The phosphole species possess the following prominent features affecting their structures, electronic properties, and reactivity [103]: (1) the phosphorus center adopts a *trigonal pyramidal geometry* due to insufficient n−π orbital interaction; (2) the phosphole LUMO lies *at a lower energy* compared to the pyrrole LUMO due to the effective σ*(P−R)−π*(1,3-diene) hyperconjugative interaction; (3) orbital energies of the phosphole π-system are easily tunable by chemical modification (metal-coordination, oxygenation, alkylation, etc.) at the phosphorus center; (4) the P-bridged 1,3-diene unit is rigid, *electron rich and polarizable*. These prominent features of phospholes originate from the intrinsic nature of the P *3s* and *3p* orbitals. Thus, the incorporation of a P-atom in the porphyrin core is a promising strategy for tuning the optical, electrochemical, and coordinating properties as well as reactivity of porphyrin species, because the phosphole subunit behaves both as a neutral P ligand and as a 1,3-dienic π-system capable of conjugation with other chemical bonds.

So farno studies of a free porphyrin or its metal complex(es) with *all pyrrole nitrogens* (P_4-porphyrins) replaced with phosphorus atoms have been performed. Based on the previous studies of porphyrin derivatives with only partial replacement of pyrrole nitrogens with P-atoms and on our current results for $NiP(P)_4$, we can formulate, for the beginning, just a few of many theoretically and practically interesting questions for future studies: What structures will P_4-porphyrins and their metal complexes adopt? How will sizes, oxidation states, and spins of metal centers influence their geometries and electronic properties? How will charges be distributed in these compounds? How will the complete replacement of pyrrole nitrogens affect the spin state of the P_4-porphyrins? How strong will different metals interact with P_4-porphyrins and how stable those compounds would be compared to tetrapyrrole compounds? How will the annulation with various aromatic/nonaromatic rings influence structures and properties of P_4-porphyrins and their metal complexes?

It would definitely be of significant interest to synthesize and characterize such compounds and investigate their structures, electronic and optical properties, and reactivities. Further theoretical studies of $NiP(P)_4$ and $P(P)_4$ derivatives are in progress.

5. Conclusions and perspectives

We performed first systematic DFT study of the effects on geometries and electronic structure (including HOMO–LUMO energy gaps, IP_v and EA_v) of the Ni-porphyrin of the following factors:

(a) simple *meso*- and β-substituents acting as inductive donors (CH_3), inductive acceptors that are electron-donating through resonance (Br), inductive electron acceptors (CF_3), and resonance enabled acceptors (NO_2); and (b) *complete replacement of pyrrole nitrogens* with phosphorus atoms. Table 11 summarizes calculated energies of frontier orbitals and derived values for all species studied in this paper.

The principal results of the study are:

1. For the bare Ni-porphyrin, inclusion of solvents effects in the calculations was found not to affect the HOMO–LUMO energy gaps but to change the IP_v and EA_v noticeably.

2. For *meso*-/β-substituted Ni-porphyrins, in the series 'inductive donors (CH_3)' → 'inductive acceptors electron-donating through resonance (Br)' → 'inductive electron acceptors (CF_3)' → 'resonance enabled acceptors (NO_2)' the HOMO–LUMO energy gaps, IP_v, and EA_v increase. The effect of β-sub-stituents on IP_v and EA_v is much more pronounced. The most pronounced structural changes occur in the Ni—N bond distances with all four types of *meso*-substituents and with two acceptor-types of β-substituents. In the series of both *meso*-and β-substituents, the ruffling distortion of the porphyrin core is retained, and becomes stronger for the two acceptor-type groups. In general, *effects of meso-substituents on the ruffling distortion of the porphyrin core is more pronounced*. Frontier MOs analysis shows that both *meso*- and β-substit-uents generally increase bonding Ni—N interactions.

3. Most significantly, *complete replacement of pyrrole nitrogens in the NiP with phosphorus atoms* was found to produce the species, $NiP(P)_4$, with the unusual structural and electronic features drastically different from the original NiP. This implies that $NiP(P)_4$ can possess interesting novel properties, including aromaticity and reactivity, leading to its various potential applications. Furthermore, $NiP(P)_4$ high stability both in the gas phase and different solvents was shown, implying the feasibility of its synthesis. These results give rise to the following very interesting research perspectives, from both theoretical and experimental points of view:

    i. to find out which $MP(P)_4$ compounds (with different metal M) are stable and can be potentially synthesized;

    ii. to investigate how $MP(P)_4$ stability, structures, and electronic properties (frontier orbital energies and shapes, HOMO–LUMO energy gaps, ionization potentials, and electron affinities) are influenced by the nature of M center (transition metal, main-group metal, nonmetal), size of M center, oxidation and spin state of M, total charge of $MP(P)_4$ species, *meso*- and β-substituents, both electron-withdrawing and electron-donating, annulation of the porphyrin ring with other aromatic cycles (benzo, naph-tho, etc.) and with nonaromatic rings, and substitution of carbons in *meso*-positions of the porphyrin ring by heteroatoms (N and P).

The following noticeable features of $MP(P)_4$ species, exemplified by $NiP(P)_4$, would make them quite different from parent MP compounds: (i) very strong $MP(P)_4$ geometry distortions, even without bulky substituents or linkers between atoms located on the opposite sites of the porphyrin moiety; (ii) charge distribution opposite to that in MP species; (iii) stabilization of the $MP(P)_4$ LUMOs compared to the MP LUMOs causing noticeable HOMO/LUMO gaps closing and thus changes of the $MP(P)_4$ redox properties compared to MP species; (iv) electron-richness and possible polarizability of $MP(P)_4$ species. These intrinsic features of $MP(P)_4$ species can put forward their potential applications in light-harvesting systems or in dye-synthesized solar cells, similar to tetrapyrrole species; in catalysis; in donoracceptor complexes with fullerenes; in 2D and 3D nanoclusters made of the $MP(P)_4$ species, where MP(P)4 units are connected via covalent or noncovalent linkages, with potential applications in catalysis, light harvesting, and photovoltaics.

Supplementary Material

Refer to Web version on PubMed Central for supplementary material.

Acknowledgments

This work was supported by the National Institute of Health (GM-048043). The authors express their gratitude to Professor David N. Beratan for invaluable help in writing this paper.

References

1. Dolphin, D., editor. The Porphyrins. Vol. I–VII. Academic; New York: 1978.
2. Lever, ABP.; Gray, HB., editors. Iron Porphyrin. Addison-Wesley Publishing Company, Inc.; Reading, MA: 1983.
3. Kadish, KM.; Smith, KM.; Guilard, R. The Porphyrin Handbook. Academic Press; San Diego, CA: 2000.
4. Hill, HAO.; Sadler, PJ.; Thomson, AJ. Metal Sites in Proteins and Models. Iron Centres, Springer-Verlag; Berlin, Heidelberg, Germany: 1997.
5. Bertini, I.; Gray, HB.; Lippard, SJ.; Valentine, JS. Bioinorganic Chemistry. University Science Book; CA: 1994.
6. Severance S, Hamza I. Trafficking of heme and porphyrind in metazoa. Chem Rev. 2009; 109:4596–4616. and references therein. [PubMed: 19764719]
7. Kitanishi K, Igarashi J, Hayasaka K, Hikage N, Saiful I, Yamauchi S, Uchida T, Ishimori K, Shimizu T. Heme-binding characteristics of the isolated PAS-A domain of mouse Per2, a transcriptional regulatory factor associated with circadian rhythms. Biochemistry. 2008; 47:6157–6168. [PubMed: 18479150]
8. Mense SM, Zhang L. Heme: a versatile signaling molecule that modulates the activity of diverse regulators ranging from transcriptional factors to MAP kinases. Cell Res. 2006; 16:681–692. [PubMed: 16894358]
9. Sheldon, RA., editor. Metalloporphyrins in Catalytic Oxidation. Marcel Dekker; New York: 1994.
10. Mansuy D. Activation of alkanes: the biomimetic approach. Coord Chem Rev. 1993; 125:129–141.
11. Kadish, KM.; Smith, KM.; Guilard, R. Handbook of Porphyrin, Science with Applications to Chemistry, Physics, Materials Science, Engineering, Biology and Medicine. Vol. III. World Scientific; Singapore: 2010.
12. Lomova, TN.; Klyueva, ME.; Klyuev, MV. The mechanism of catalytic action of the coordination centres of catalase synthetic models. In: Lomova, TN.; Zaikov, GE., editors. Chemical Processes with Participation of Biological and Related Compounds. Koninklijke Brill NV; Leiden, The Netherlands: 2008. p. 93-116.
13. Che CM, Huang JS. Metalloporphyrin-based oxidation systems: from biomimetic reactions to application in organic synthesis. Chem Commun. 2009:3996–4015.
14. Senge MO, Fazekas M, Notaras EGA, Blau WJ, Zawadzka M, Locos OB, Ni Mhuircheartaigh EM. Nonlinear optical properties of porphyrins. Adv Mater. 2007; 19:2737–2774.
15. Gust D, Moore TA, Moore AL. Mimicking photosynthetic solar energy transduction. Acc Chem Res. 2001; 34:40–48. [PubMed: 11170355]
16. Guldi DM. Fullerene–porphyrin architectures; photosynthetic antenna and reaction center models. Chem Soc Rev. 2002; 31:22–36. [PubMed: 12108980]
17. Wasielewski MR. Self-assembly strategies for integrating light harvesting and charge separation in artificial photosynthetic systems. Acc Chem Res. 2009; 42:1910–1921. [PubMed: 19803479]
18. Aratani N, Kim D, Osuka A. Discrete cyclic porphyrin arrays as artificial light-harvesting antenna. Acc Chem Res. 2009; 42:1922–1934. [PubMed: 19842697]
19. Imanori H, Umeyama T, Ito S. Large π-aromatic molecules as potential sensitizers for highly efficient dye-sensitized solar cells. Acc Chem Res. 2009; 42:1809–1818. [PubMed: 19408942]
20. Planells M, Forneli A, Martínez-Ferrero E, Sánchez-Díaz A, Sarmentero MA, Ballester P, Palomares E, O'Regan BC. The effect of molecular aggregates over the interfacial charge transfer processes on dyesensitized solar cells. Appl Phys Lett. 2008; 92:153506.
21. Ma R, Guo P, Yang L, Guo L, Zhang X, Nazeeruddin MK, Grätzel M. Theoretical screening of —NH_2—, —OH—, —CH_3—, —F—, and —SH-substituted porphyrins as sensitizer candidates for dye-sensitized solar cells. J Phys Chem A. 2010; 114:1973–1979. and references therein. [PubMed: 20067227]
22. Youngblood WJ, Lee SHA, Maeda K, Mallouk TE. Visible light water splitting using dye-sensitized oxide semiconductors. Acc Chem Res. 2009; 42:1966–1973. [PubMed: 19905000]

23. Monti D, Nardis S, Stefanelli M, Paolesse R, Di Natale C, D'Amico A. Porphyrin-based nanostructures for sensing application. J Sensors. 2009:1–10.
24. Zhu Y, Silverman RB. Electronic effects of peripheral substituents atporphyrin meso positions. J Org Chem. 2007; 72:233–239. [PubMed: 17194104]
25. Jux N. The porphyrin twist: Hückel and Möbius aromaticity. Angew Chem Int Ed. 2008; 47:2543–2546.
26. Krygowski TM, Cyrański MK. Structural aspects of aromaticity. Chem Rev. 2001; 101:1385–1420. [PubMed: 11710226]
27. Cyrański MK, Krygowski TM, Wisiorowski M, Hommes NJR, Schleyer PvR. Global and local aromaticity in porphyrins: an analysis based onmolecular geometries and nucleus-independent chemical shifts. Angew Chem Int Ed. 1998; 37:177–180.
28. Feixas F, Sola M, Swart M. Chemical bonding and aromaticity in metalloporphyrins. Can J Chem. 2009; 87:1063–1073.
29. Bikiel DE, Forti F, Boechi L, Nardini M, Luque FJ, Marti MA, Estrin DA. Role of heme distortion on oxygen affinity in heme proteins: the protoglobin case. J Phys Chem B. 2010; 114:8536–8543. [PubMed: 20524694]
30. Shelnutt, JA. Molecular simulations and normal-coordinate structural analysis of porphyrins and heme proteins. In: Kadish, KM.; Smith, KM.; Guilard, R., editors. The Porphyrin Handbook. Vol. 7. Academic Press; San Diego, CA: 2000. p. 167-224.
31. Jentzen W, Ma JG, Shelnutt JA. Conservation of the conformation of the porphyrin macrocycle in heme proteins. Biophys J. 1998; 74:753–763. and references therein. [PubMed: 9533688]
32. Jentzen W, Simpson MC, Hobbs JD, Song XZ, Ema T, Nelson NY, Medforth CJ, Smith KM, Veyrat M, Mazzanti M, Ramasseul R, Marchon JC, Takeuchi T, Goddard WA III, Shelnutt JA. Ruffling in a series of nickel(II) meso-tetrasubstituted porphyrins as a model for the conserved ruffling of the heme of cytochromes c. J Am Chem Soc. 1995; 117:11085–11097.
33. Jentzen W, Song XZ, Shelnutt JA. Structural characterization of synthetic and protein-bound porphyrins in terms of the lowest-frequency normal coordinates of the macrocycle. J Phys Chem B. 1997; 101:1684–1699.
34. Scheidt, WR. Systematic of stereochemistry of porphyrins and metalloporphyrins. In: Kadish, KM.; Smith, KM.; Guilard, R., editors. The Porphyrin Handbook. Vol. 3. Academic Press; San Diego, CA: 2000. p. 49-112.
35. Walker FA. Models of the bis-histidine-ligated electron-transferring cytochromes. Comparative geometric and electronic structure of low-spin ferro- and ferrihemes. Chem Rev. 2004; 104:589–616. and references therein. [PubMed: 14871136]
36. Neya S, Suzuki M, Hoshino T, Ode H, Imai K, Komatsu T, Ikezaki A, Nakamura M, Furutani Y, Kandori H. Molecular insight into intrinsic heme distortion in ligand binding in hemoprotein. Biochemistry. 2010; 49:5642–5650. [PubMed: 20536131]
37. Nakamura M, Ohgo Y, Ikezaki A. Electronic ground states of low-spin iron(III) porphyrinoids. J Inorg Biochem. 2008; 102:433–445. [PubMed: 18171587]
38. Nakamura M. Electronic structures of highly deformed iron(III) porphyrin complexes. Coord Chem Rev. 2006; 250:2271–2294.
39. Shao J, Steene E, Hoffman BM, Ghosh A. EPR, ENDOR, and DFT studies on (β-octahalo-meso-tetraarylporphyrin)copper complexes: characterization of the metal(d_{x2-y2})-porphyrin(a_{2u}) orbital interaction. Eur J Inorg Chem. 2005:1609–1615.
40. Patra R, Chaudhury A, Ghosh SK, Rath SP. Modulation of metal displacements in a saddle distorted macrocycle: synthesis, structure, and properties of high-spin Fe(III) porphyrins and implications for hemoproteins. Inorg Chem. 2008; 47:8324–8335. [PubMed: 18700752]
41. Ghosh SK, Patra R, Rath SP. Axial ligand coordination in sterically strained vanadyl porphyrins: synthesis, structure, and properties. Inorg Chem. 2008; 47:9848–9856. [PubMed: 18823111]
42. Patra R, Bhowmik S, Ghosh SK, Rath SP. The effect of steric crowding on porphyrin conformation and ring orientations in a series of iron(III) μ-oxodimers containing meso-nitrooctaethylporphyrins. Eur J Inorg Chem. 2009:654–665.

43. Ghosh SK, Patra R, Rath SP. Remarkably bent, ethane-linked, diiron(III) μ-oxobisporphyrin: synthesis, structure, conformational switching, and photocatalytic oxidation. Inorg Chem. 2008; 47:10196–10198. [PubMed: 18921994]
44. Liptak MD, Wen X, Bren KL. NMR and DFT investigation of heme ruffling: functional implications for cytochrome c. J Am Chem Soc. 2010; 132:9753–9763. [PubMed: 20572664]
45. Shelnutt JA, Song XZ, Ma JA, Jia SJ, Jentzen W, Medforth CJ. Nonplanar porphyrins and their significance in proteins. Chem Soc Rev. 1998; 27:31–41. and references therein.
46. Hoard JL. Stereochemistry of hemes and other metalloporphyrins. Science. 1971; 174:1295–1302. [PubMed: 4332625]
47. Hoard JL. Some aspects of metalloporphyrin stereochemistry. Ann NY Acad Sci. 1973; 206:18–31. [PubMed: 4518386]
48. Hoard, JL. Stereochemistry of porphyrins and metalloporphyrins. In: Smith, KM., editor. Porphyrins and Metalloporphyrins. Elsevier; Amsterdam: 1975. p. 317-380.
49. Senge MO. Exercises in molecular gymnastics - bending, stretching and twisting porphyrins. Chem Commun. 2006:243–256.
50. Röder B, Büchner M, Rückmann I, Senge MO. Correlation of photophysical parameters with macrocycle distortions in porphyrins with graded degree of saddle distortion. Photochem Photobiol Sci. 2010; 9:1152–1158. [PubMed: 20571638]
51. CRC Handbook of Chemistry and Physics (81). :2000–2001.
52. Stoll LK, Zgierski MZ, Kozlowski PM. Density functional theory analysis of nickel octaethylporphyrin ruffling. J Phys Chem A. 2002; 106:170–175.
53. Kozlowski PM, Bingham JR, Jarzecki AA. Theoretical analysis of core size effects inmetalloporphyrins. J Phys Chem A. 2008; 112:12781–12788. [PubMed: 18754605]
54. Kozlowski PM, Rush TS III, Jarzecki AA, Zgierski MZ, Chase B, Piffat C, Ye BH, Li XY, Pulay P, Spiro TG. DFT-SQM force field for nickel porphine: intrinsic ruffling. J Phys Chem A. 1999; 103:1357–1366.
55. Hirao H, Shaik S, Kozlowski PM. Theoretical analysis of the structural and electronic properties of metalloporphyrin π-cation radicals. J Phys Chem A. 2006; 110:6091–6099. [PubMed: 16671680]
56. Yoshizawa K, Nakayama T, Kamachi T, Kozlowski PM. Vibronic interaction in metalloporphyrin π-anion radicals. J Phys Chem A. 2007; 111:852–857. [PubMed: 17266225]
57. Stoll LK, Zgierski MZ, Kozlowski PM. Infrared spectra of nickel octaethylporphyrin and its isotopomers computed via density functional theory-scaled mechanical (DFT-SQM) method. J Phys Chem A. 2003; 107:4165–4171.
58. Rush TS III, Kozlowski PM, Piffat CA, Kumble R, Zgierski MZ, Spiro TG. Computational modeling of metalloporphyrin structure and vibrational spectra: porphyrin ruffling in NiTPP. J Phys Chem B. 2000; 104:5020–5034.
59. Liao MS, Scheiner S. Electronic structure and bonding in metal porphyrins, metal = Fe, Co, Ni, Cu, Zn. J Chem Phys. 2002; 117:205–219.
60. Liao MS, Scheiner S. Comparative study of metal–porphyrins, –porphyrazines, and –phthalocyanines. J Comput Chem. 2002; 23:1391–1403. [PubMed: 12370942]
61. Zwaans R, van Lenthe JH, den Boer DHW. Ab initio calculations on first-row transition metal porphyrins. Part 2. Ground state spin multiplicities, calculated ionization potentials and electron affinities and their relation to catalytic activity. J Mol Struct (Theochem). 1996; 367:15–24.
62. Zwaans R, van Lenthe JH, den Boer DHW. Ab initio calculations on first-row transition metal porphyrins. Part 1. Geometrical details, charge distributions and the effects of additional charge. J Mol Struct (Theochem). 1995; 339:153–160.
63. Stoyanov SR, Yin CX, Gray MR, Stryker JM, Gusarov S, Kovalenko A. Computational and experimental study of the structure, binding preferences, and spectroscopy of nickel(II) and vanadyl porphyrins in petroleum. J Phys Chem B. 2010; 114:2180–2188. [PubMed: 20099931]
64. Feng XT, Yu JG, Lei M, Fang WH, Liu S. Towards understanding metal-binding specificity of porphyrin: a conceptual density functional theory study. J Phys Chem B. 2009; 113:13381–13889. [PubMed: 19751061]

65. Feng XT, Yu JG, Liu RZ, Lei M, Fang WH, De Proft F, Liu S. Why iron? A spin-polarized conceptual density functional theory study on metal-binding specificity of porphyrin. J Phys Chem A. 2010; 114:6342–6349. [PubMed: 20450212]
66. Peralta GA, Seth M, Ziegler T. Magnetic circular dichroism of porphyrins containing M = Ca, Ni, and Zn: a computational study based on time-dependent density functional theory. Inorg Chem. 2007; 46:9111–9125. [PubMed: 17914806]
67. Rosa A, Ricciardi G, Baerends EJ, Zimin M, Rodgers MAJ, Matsumoto S, Ono N. Structural, optical, and photophysical properties of nickel(II) alkylthioporphyrins: insights from experimental and DFT/TDDFT studies. Inorg Chem. 2005; 44:6609–6622. [PubMed: 16156618]
68. Evans JS, Musselman RL. Red shifting due to nonplanarity in alkylporphyrins: solid-state polarized UV–vis spectra and ZINDO calculations of two nickel(II)octaethylporphyrins. Inorg Chem. 2004; 43:5613–5629. [PubMed: 15332813]
69. Rosa A, Ricciardi G, Baerends EJ, van Gisbergen SJA. The optical spectra of NiP. NiPz, NiTBP, and NiPc: electronic effects of meso-tetraaza substitution and tetrabenzo annulation. J Phys Chem A. 2001; 105:3311–3327.
70. Ryeng H, Ghosh A. Do nonplanar distortions of porphyrins bring about strongly red-shifted electronic spectra? Controversy, consensus, new developments, and relevance to chelatases. J Am Chem Soc. 2002; 124:8099–8103. [PubMed: 12095355]
71. DiMagno SG, Wertsching AK, Ross CR II. Electronic consequences of nonplanar core conformations in electron-deficient porphyrins: the structure and spectroscopic properties of [5,10,15,20-tetrakis(heptafluoropropyl) porphinato]cobalt(III). J Am Chem Soc. 1995; 117:8279–8280.
72. Patchkovskii S, Kozlowski PM, Zgierski MZ. Theoretical analysis of singlet and triplet excited states of nickel porphyrins. J Chem Phys. 2004; 121:1317–1324. [PubMed: 15260674]
73. Zamyatin AV, Soldatova AV, Rodgers MAJ. The photophysics of Ni(II) meso-tetraphenylbenzoporphyrin: a combined theoretical and experimental investigation. Inorg Chim Acta. 2007; 360:857–868.
74. Guo L, Ellis DE, Hoffman BM, Ishikawa Y. Ligand substitution effect on electronic structure and optical properties of nickel porphyrazines. Inorg Chem. 1996; 35:5304–5312.
75. Song Y, Haddad RE, Jia SL, Hok S, Olmstead MM, Nurco DJ, Schore NE, Zhang J, Ma JG, Smith KM, Gazeau S, Pecaut J, Marchon JC, Medforth CJ, Shelnutt JA. Energetics and structural consequences of axial ligand coordination in nonplanar nickel porphyrins. J Am Chem Soc. 2005; 127:1179–1192. [PubMed: 15669857]
76. Schweitzer-Stenner R, Lemke C, Haddad R, Qiu Y, Shelnutt JA, Quirke JME, Dreybrodt W. Conformational distortions of metalloporphyrins with electron-withdrawing NO_2 substituents at different meso positions. A structural analysis by polarized resonance Raman dispersion spectroscopy and molecular mechanics calculations. J Phys Chem A. 2001; 105:6680–6694.
77. Alden RG, Crawford BA, Doolen R, Ondrias MR, Shelnutt JA. Ruffling of nickel(II) octaethylporphyrin in solution. J Am Chem Soc. 1989; 111:2070–2072.
78. Alden RG, Ondrias MR, Shelnutt JA. Influences of π–π complex formation, dimerization, and binding to hemoglobin on the planarity of nickel(II) porphyrins. J Am Chem Soc. 1990; 112:691–697.
79. Anderson KK, Hobbs JD, Luo L, Stanley KD, Quirke JME, Shelnutt JA. Planar-nonplanar conformational equilibrium in metal derivatives of octaethylporphyrin and meso-nitro octaethylporphyrin. J Am Chem Soc. 1993; 115:12346–12352.
80. Shelnutt JA, Ortiz V. Substituent effects on the electronic structure of metalloporphyrins: a quantitative analysis in terms of four-orbital-model parameters. J Phys Chem. 1985; 89:4733–4739.
81. Delaere D, Nguyen MT. A density functional study of the ground state electronic structure of phosphorus-porphyrins. Chem Phys Lett. 2003; 376:329–337.
82. Matano Y, Nakabuchi T, Imahori H. Synthesis, structures, and aromaticity of phosphole-containing porphyrins and their metal complexes. Pure Appl Chem. 2010; 82:583–593.

83. Nakabuchi T, Matano Y, Imahori H. Remarkable effects of P-perfluorophenyl group on the synthesis of core-modified phosphaporphyrinoids and phosphadithiasapphyrin. Org Lett. 2010; 12:1112–1115. [PubMed: 20143844]
84. Nakabuchi T, Nakashima M, Fujishige S, Nakano H, Matano Y, Imahori H. Synthesis and reactions of phosphaporphyrins: reconstruction of π-skeleton triggered by oxygenation of a core phosphorus atom. J Org Chem. 2010; 75:375–389. [PubMed: 20000654]
85. Matano Y, Imahori H. Phosphole-containing calixpyrroles, calixphyrins, and porphyrins: synthesis and coordination chemistry. Acc Chem Res. 2009; 42:1193–1204. [PubMed: 19496532]
86. Matano Y, Nakashima M, Nakabuchi T, Imahori H, Fujishige S, Nakano H. Monophosphaporphyrins: oxidative π-extension at the peripherally fused carbocycle of the phosphaporphyrin ring. Org Lett. 2008; 10:553–556. [PubMed: 18189409]
87. Matano Y, Nakabuchi T, Fujishige S, Nakano H, Imahori H. Redox-coupled complexation of 23-phospha-21-thiaporphyrin with group 10 metals: a convenient access to stable core-modified isophorin–metal complexes. J Am Chem Soc. 2008; 130:16446–16447. [PubMed: 19554678]
88. Matano Y, Nakabuchi T, Miyajima T, Imahori H, Nakano H. Synthesis of phosphorus-containing hybrid porphyrin. Org Lett. 2006; 8:5713–5716. [PubMed: 17134254]
89. Matano Y, Miyajima T, Ochi N, Nakabuchi T, Shiro M, Nakao Y, Sakaki S, Imahori H. Syntheses, structures, and coordination chemistry of phosphole-containing hybrid calixphyrins: promising macrocyclic P,N_2,X-mixed donor ligands for designing reactive transition-metal complexes. J Am Chem Soc. 2008; 130:990–1002. [PubMed: 18161971]
90. Matano Y, Miyajima T, Nakabuchi T, Imahori H, Ochi N, Sakaki S. Phosphorus-containing hybrid calixphyrins: promising mixed-donor ligands for visible and efficient palladium catalysts. J Am Chem Soc. 2006; 128:11760–11761. [PubMed: 16953607]
91. Frisch, MJ.; Trucks, GW.; Schlegel, HB., et al. Gaussian03, Revision D.02. Gaussian, Inc.; Wallingford, CT: 2004.
92. Ditchfield R, Hehre WJ, Pople JA. Self-consistent molecular-orbital methods. IX. An extended Gaussian-type basis for molecular-orbital studies of organic molecules. J Chem Phys. 1971; 54:724–728.
93. Hehre WJ, Ditchfield R, Pople JA. Self-consistent molecular orbital methods. XII. Further extensions of Gaussian-type basis sets for use in molecular orbitalstudies of organic molecules. J Chem Phys. 1972; 56:2257–2261.
94. Hariharan PC, Pople JA. Accuracy of AH_n equilibrium geometries by single determinant molecular orbital theory. Mol Phys. 1974; 27:209–214.
95. Gordon MS. The isomers of silacyclopropane. Chem Phys Lett. 1980; 76:163–168.
96. Hariharan PC, Pople JA. The influence of polarization functions on molecular orbital hydrogenation energies. Theo Chim Acta. 1973; 28:213–222.
97. Parr, RG.; Yang, W. Density-Functional Theory of Atoms and Molecules. Oxford University Press; Oxford: 1989.
98. Cances E, Mennucci B, Tomasi J. A new integral equation formalism for the polarizable continuum model: theoretical background and applications to isotropic and anisotropic dielectrics. J Chem Phys. 1997; 107:3032–3041.
99. Varetto, U. Molekel 5.4.0.8. Swiss National Supercomputing Centre; Manno (Switzerland):
100. Jentzen W, Turowska-Tyrk I, Scheidt WR, Shelnutt JA. Planar solid-state and solution structures of (porphinato)nickel(II) as determined by X-ray diffraction and resonance Raman spectroscopy. Inorg Chem. 1996; 35:3559–3567.
101. Kadish, KM.; Smith, KM.; Guilard, R. The Porphyrin Handbook. Vol. 8. Academic Press; San Diego, CA: 2000.
102. Khandelwal SC, Roebber JL. The photoelectron spectra of tetraphenylporphine and some metallotetraphenylporphyrins. Chem Phys Lett. 1975; 34:355–359.
103. Matano Y, Imahori H. Design and synthesis of phosphole-based π systems for novel organic materials. Org Biomol Chem. 2009; 7:1258–1271. [PubMed: 19300806]

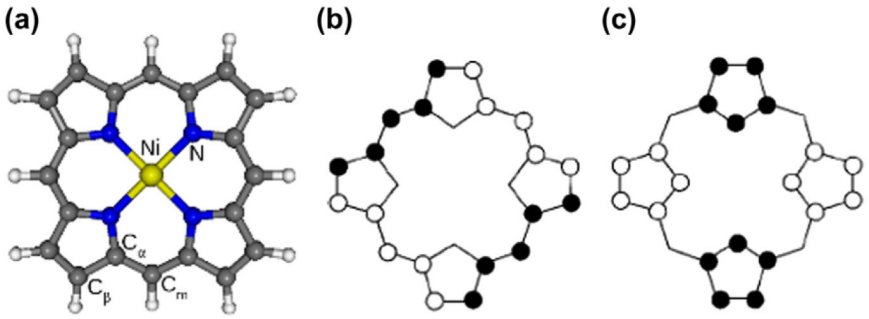

Fig. 1.

Ni-porphyrin structure and atom labeling scheme (a), and schematic depiction of ruffled (b) and saddled (c) porphyrin conformations. The filled and open circles indicate displacements on opposite sides of the mean plane of the porphyrin ring.

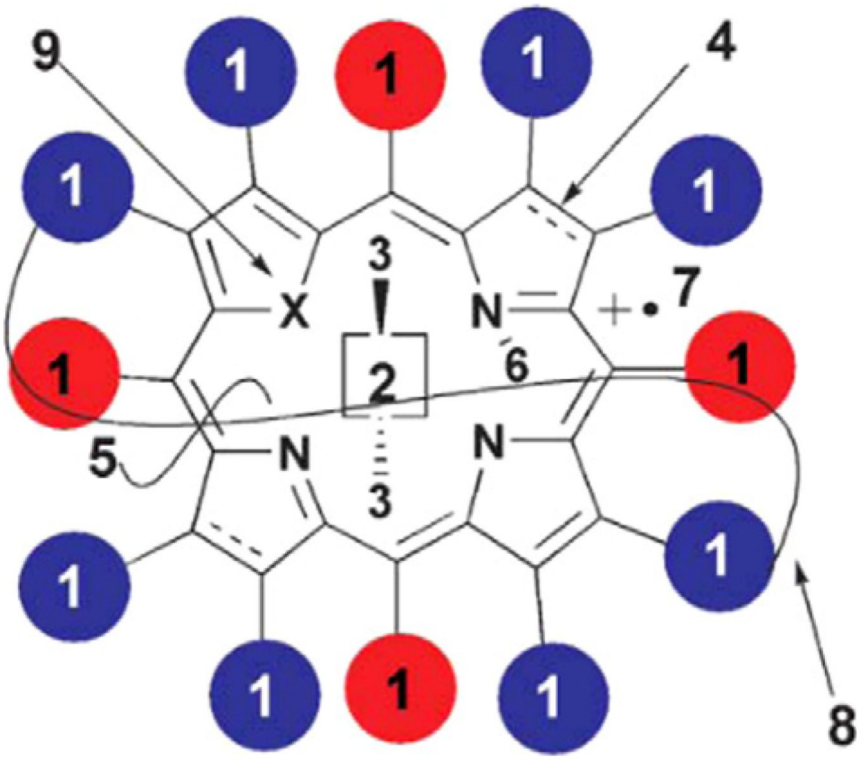

Fig. 2.

Factors capable of causing distortions of the porphyrin macrocycle from planarity: (1) sterically demanding substituents (white and black “1”'s refer to β-and *meso*-substituents, respectively); (2) metal center oxidation/spin state; (3) axial ligands; (4) oxidation/reduction; (5) altering conjugation; (6) N-substitution; (7) cationradical formation; (8) strapping” of the macrocycle via covalent linkage of the *meso*- or β-pyrrole positions; (9) heteroatom substitution [49,50].

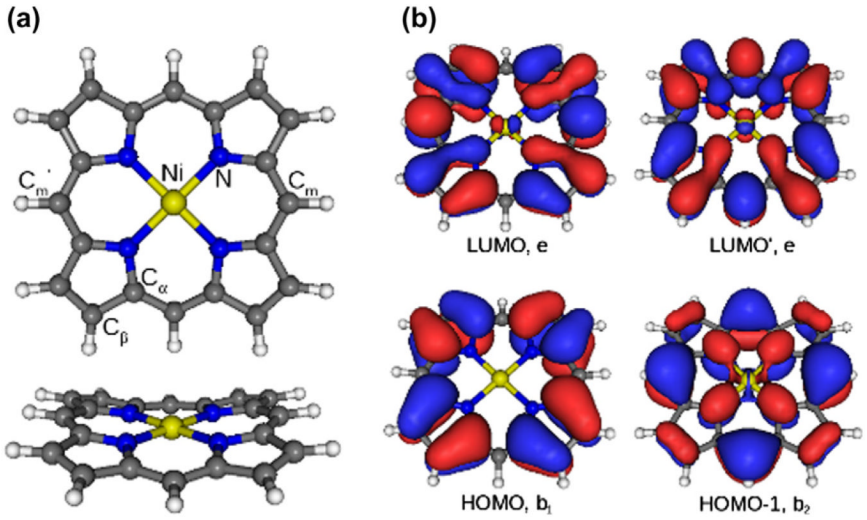

Fig. 3.
Structure of the global minimum bare NiP (D_{2d}, $^1A_1$) (a), two HOMOs and two LUMOs of the NiP structure (b).

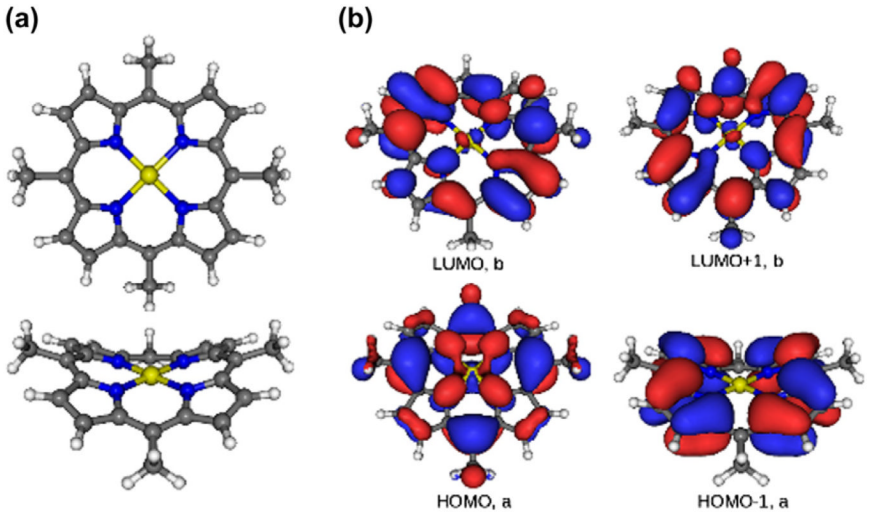

Fig. 4.
Structure of the global minimum NiP(*meso*-CH_3)$_4$ (C_2, ^{1}A) (a), its two HOMOs and two LUMOs (b).

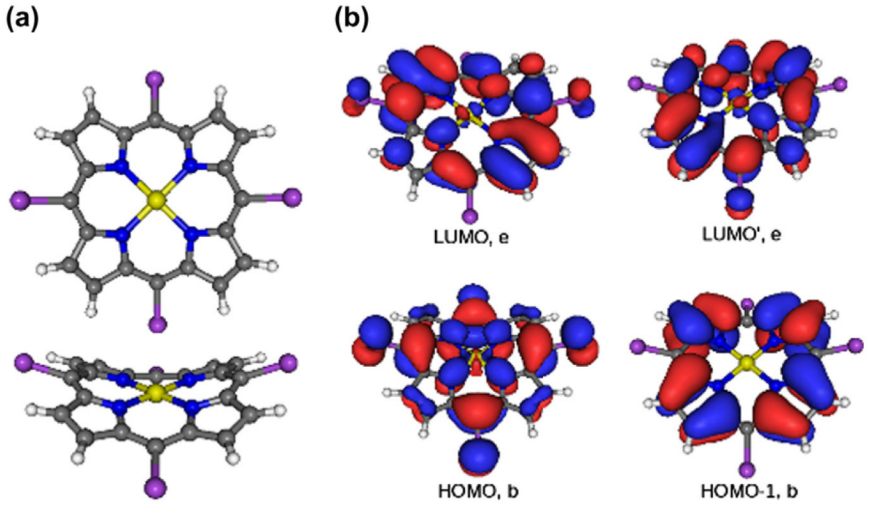

Fig. 5.
Structure of the global minimum NiP(*meso*-Br)$_4$ (S_4, ^{1}A) (a), two HOMOs and two LUMOs of NiP(*meso*-Br)$_4$ (b).

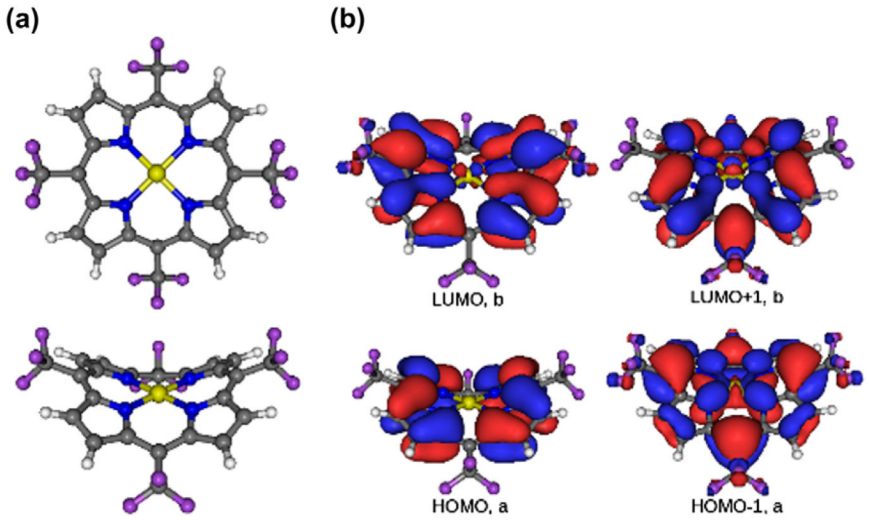

Fig. 6.

Structure of the global minimum NiP(*meso*-CF_3)$_4$ (C_2, ^{1}A) (a), two HOMOs and two LUMOs of NiP(*meso*-CF_3)$_4$ (b).

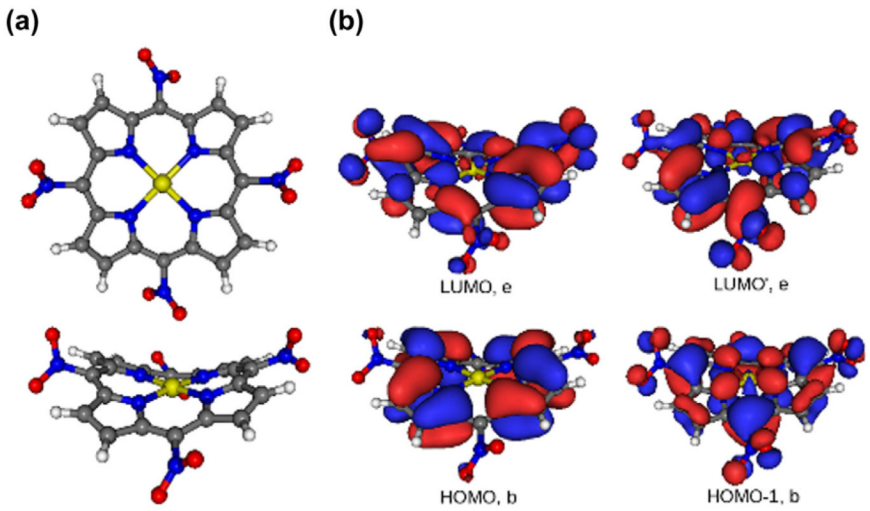

Fig. 7.
Structure of the global minimum NiP(*meso*-NO_2)$_4$ (S_4, ^{1}A) (a), two HOMOs and two LUMOs of NiP(*meso*-NO_2)$_4$ (b).

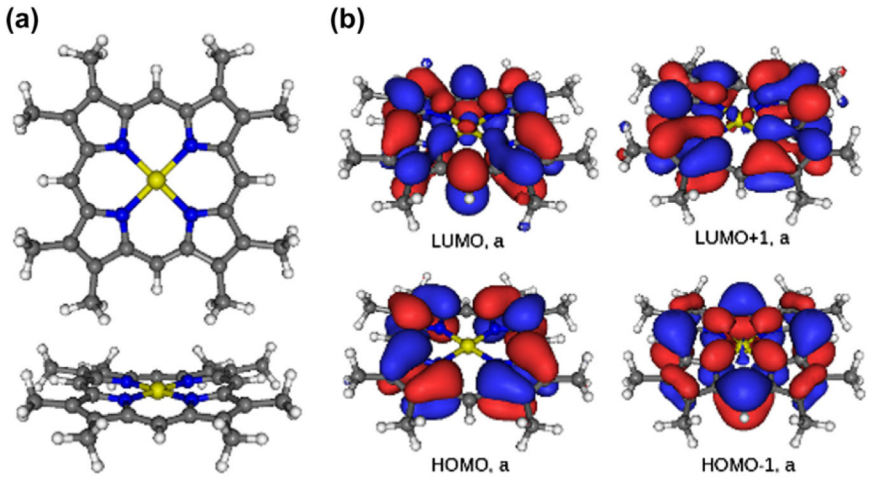

Fig. 8.
Structure of global minimum NiP(β-CH_3)$_8$ (C_1, ^{1}A) (a), two HOMOs and two LUMOs of NiP(β-CH_3)$_8$ (b).

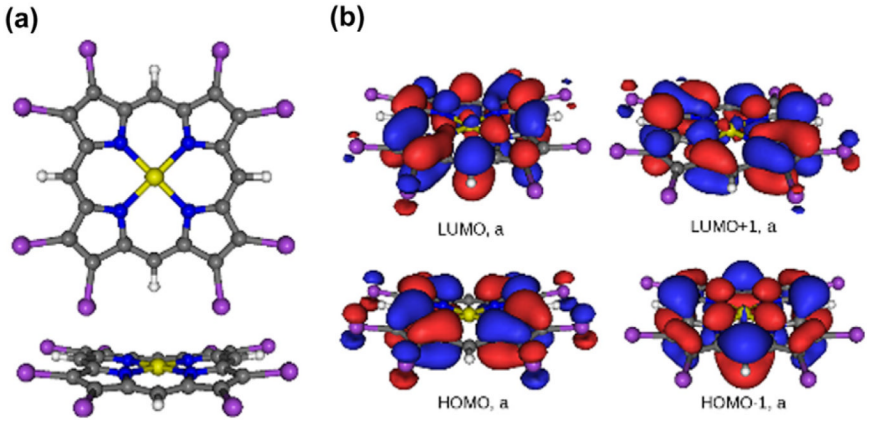

Fig. 9.
Structure of the global minimum NiP(β-Br)$_8$ (C_1, ^{1}A) (a), two HOMOs and two LUMOs of NiP(β-Br)$_8$ (b).

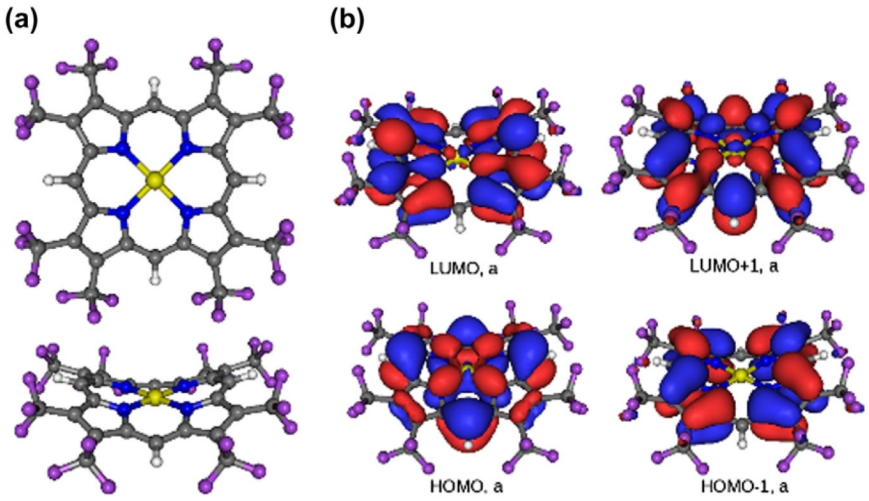

Fig. 10.
Structure of the global minimum NiP(β-CF_3)$_8$ (C_1, ^{1}A) (a), two HOMOs and two LUMOs of NiP(β-CF_3)$_8$ (b).

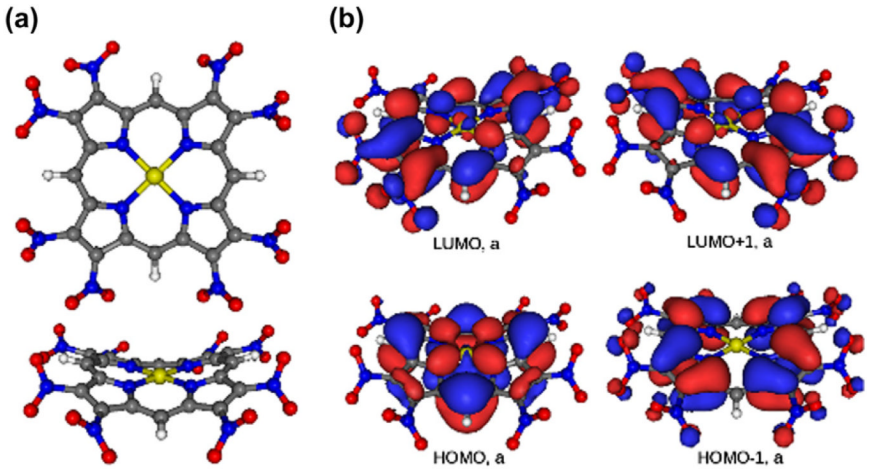

Fig. 11.
Structure of the global minimum NiP(β-NO_2)$_8$ (C_1, ^{1}A) (a), two HOMOs and two LUMOs of NiP(β-NO_2)$_8$ (b).

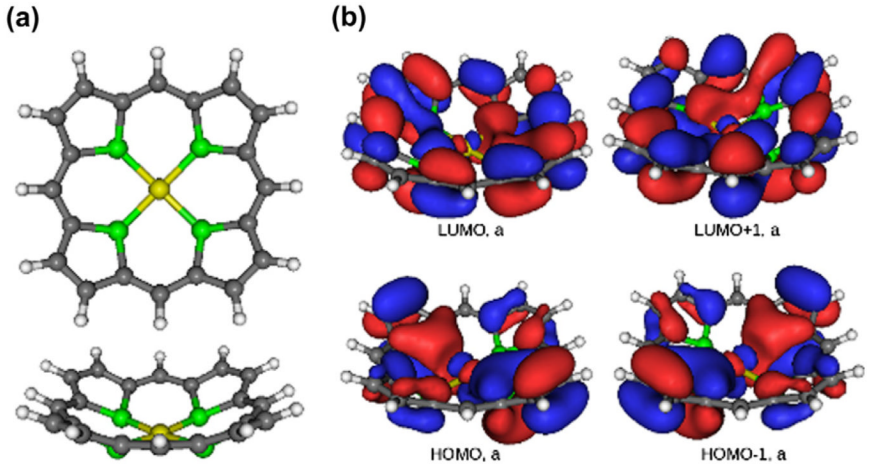

Fig. 12.
Structure of the global minimum $NiP(P)_4$ (C_2, ^1A) (a), its two HOMOs and two LUMOs (b).

Table 1

Calculated and experimental structural parameters of the NiP species ((D_{2d}, $^1A_1$) and(C_1, ^3A) (in parentheses)).

Bond length, Å/angles, deg.	Calculated, gas phase	Exp.[a]
Ni—N	1.94 (2.02)	1.951(2)
N—C_α	1.38 (1.37; 1.38)	1.379(2)
C_α—C_β	1.44 (1.44; 1.45)	1.435(4)
C_β—C_β	1.36 (1.36)	1.347(3)
C_α—C_m	1.38 (1.39)	1.371(3)
C_m—H	1.09 (1.09)	–
C_β—H	1.08 (1.08)	–
$C_m–Ni–C_m'$ [b]	167.5 (180.0)	–
C_α—C_m—C_α	123.1 (125.7)	123.5(2)
C_α—N—C_α	104.5 (106.0)	–

[a] Selected structural parameters are provided for monoclinic NiP [100], numbers in parentheses are the estimated standard deviations.

[b] *Meso*-carbons are located at the opposite sides of the porphyrin core, see Figs. 1a and 3a.

Table 2

NiP species Mulliken charges/spins, e ((D_{2d}, $^1A_1$) and (C_1,^3A) (in parentheses)).

Atom	Mulliken charge/spin
Ni	0.79 (0.92/1.73)
N	−0.71 (−0.74/0.05; −0.76/0.05)
C_α	0.37 (0.38/0.0; 0.38/0.01)
C_β	−0.18 (−0.18/0.0; −0.18/0.01)
C_m	−0.28 (−0.28/0.0)
C_β—H	0.14 (0.14/0.0)
C_m—H	0.14 (0.14/0.0)

Table 3

Calculated structural parameters of the *meso*-substituted NiP species in the gas phase.

Bond length, Å/angles, deg.	**Substituting group (XY_n)**			
	CH_3	**Br**	**CF_3**	**NO_2**
Ni—N	1.91	1.92	1.89	1.92
N—C_α	1.38	1.38	1.38	1.38
C_α—C_β	1.44	1.44	1.45	1.44
C_β—C_β	1.36	1.36	1.36	1.36
C_α—C_m	1.40	1.39	1.40	1.39
C_m—X	1.51	1.91	1.51	1.47
X—Y	1.09; 1.10	–	1.35	1.23
C_β—H	1.08	1.08	1.08	1.08
$C_m-Ni-C'_m$	156.4	157.4	150.6	157.7
C_α—C_m—C_α	120.2	123.5	121.2	124.3
C_α—N—C_α	105.9	104.9	106.3	104.9

Table 4

Meso-substituted NiP species Mulliken charges, e (gas phase).

Atom	Substituting group (XY_n)			
	CH_3	Br	CF_3	NO_2
Ni	0.76	0.80	0.78	0.81
N	−0.71	−0.72	−0.72	−0.74
C_α	0.31	0.34	0.32	0.36, 0.37
C_β	−0.18	−0.17	−0.17	−0.15, −0.16
C_m	0.05	−0.06	−0.14	0.15
$X_{(subst.)}$	−0.54	−0.09	0.82	0.33
$Y_{(subst.)}$	0.16, 0.17	–	−0.26, −0.27	−0.36, −0.37
C_β—H	0.13	0.17	0.17	0.19, 0.20

Table 5

Calculated HOMO/LUMO energies (a.u.), ΔE(HOMO–LUMO) (eV), IP_v (eV) and EA_v (eV) of bare and meso-substituted NiP species (gas phase).

Species	E(HOMO/LUMO)	Δ*E*(HOMO– LUMO)	IP_v	EA_v
NiP (D_{2d}, $^1A_1$)	−0.19123/−0.07632	3.13	6.59	0.74
NiP(*meso*-CH_3)$_4$ (C_2, ^1A)	−0.17816/−0.07226	2.88	6.11	0.68
NiP(*meso*-Br)$_4$ (S_4, ^1A)	−0.20447/−0.10022	2.84	6.77	1.49
NiP(*meso*-CF_3)$_4$ (C_2, ^1A)	−0.21955/−0.11531	2.84	7.28	1.82
NiP(*meso*-NO_2)$_4$ (S_4, ^1A)	−0.24198/−0.14273	2.70	8.35	2.62

Table 6

Calculated geometrical parameters of the β-substituted NiP species in the gas phase.

Bond length, Å/angles, deg.	**Substituting group (XY_n)**			
	CH_3	**Br**	**CF_3**	**NO_2**
Ni—N	1.94	1.95	1.92	1.92; 1.93
N—C_α	1.38	1.38	1.37	1.38
C_α—C_β	1.45	1.44	1.45	1.44
C_β—C_β	1.37	1.36	1.37	1.36
C_α—C_m	1.38	1.38	1.39	1.38
C_β—X	1.50	1.87	1.51	1.45
X—Y	1.09; 1.10	–	1.35; 1.36	1.22; 1.23
C_m—H	1.08	1.08	1.08	1.08
$C_m-Ni-C'_m$	168.0; 168.1	168.1	156.3	158.7; 158.7
C_α—C_m—C_α	123.5	122.6	122.1	121.4; 121.5
C_α—N—C_α	104.3	105.2	106.3	106.5

Table 7

β-Substituted NiP species Mulliken charges, e (gas-phase).

Atom	Substituting Group (XY_n)			
	CH_3	Br	CF_3	NO_2
Ni	0.77	0.82	0.82	0.85
N	−0.74	−0.74	−0.74	−0.76
C_α	0.34	0.37	0.35	0.38
C_β	0.07	0.01	−0.12	0.27
C_m	−0.29	−0.26	−0.26	−0.22; −0.23
$X_{(subst.)}$	−0.54	−0.07	0.85	0.17
$Y_{(subst.)}$	0.16	–	−0.25; −0.26; −0.27	−0.35; −0.36
C_m—H	0.13	0.19	0.20	0.24

Table 8

Calculated HOMO/LUMO energies (a.u.), ΔE(HOMO–LUMO) (eV), IP_v (eV) and EA_v (eV) of bare and β-substituted NiP species (gas phase).

Species	HOMO/LUMO energies	ΔE(HOMO–LUMO)	IP_v	EA_v
NiP (D_{2d}, $^1A_1$)	−0.19123/−0.07632	3.13	6.59	0.74
NiP(β-CH_3)$_8$ (C_1, ^1A)	−0.17352/−0.06440	2.97	5.95	0.51
NiP(β-Br)$_8$ (C_1, ^1A)	−0.21862/−0.10945	2.97	7.08	1.84
NiP(β-CF_3)$_8$ (C_1, ^1A)	−0.24566/−0.13839	2.92	7.94	2.55
NiP(β-NO_2)$_8$ (C_1, ^1A)	−0.28301/−0.18542	2.66	8.90	3.87

Table 9

Calculated principal structural parameters of the $NiP(P)_4$ species (C_2, ^1A).

Bond length, Å/angles, deg.	Gas phase
Ni—P	2.1
P—C_α	1.8
C_α—C_β	1.4
C_β—C_β	1.8
C_α—C_m	1.4
C_m—H	1.1
C_β—H	1.1
C_m-Ni-C_m'	146.5
C_α—P—C_α	92.9

Table 10

$NiP(P)_4$ Mulliken charges, e (C_2, ^1A).

Atom	Gas phase
Ni	−0.12
P	0.26
C_α	−0.12
C_β	−0.14
C_m	−0.13
C_β—H	0.14
C_m—H	0.14

Table 11

Calculated HOMO/LUMO energies (a.u.), ΔE(HOMO–LUMO) (eV), IP_v (eV) and EA_v (eV) of all NiP species studied (gas phase).

Species	*E*(HOMO/LUMO)	Δ*E*(HOMO– LUMO)	IP_v	EA_v
NiP (D_{2d}, $^1A_1$)	−0.19123/−0.07632	3.13	6.59	0.74
NiP(*meso*-CH_3)$_4$ (C_2, ^1A)	−0.17816/−0.07226	2.88	6.11	0.68
NiP(*meso*-Br)$_4$ (S_4, ^1A)	−0.20447/−0.10022	2.84	6.77	1.49
NiP(*meso*-CF_3)$_4$ (C_2, ^1A)	−0.21955/−0.11531	2.84	7.28	1.82
NiP(*meso*-NO_2)$_4$ (S_4, ^1A)	−0.24198/−0.14273	2.70	8.35	2.62
NiP(β-CH_3)$_8$ (C_1, ^1A)	−0.17352/−0.06440	2.97	5.95	0.51
NiP(β-Br)$_8$ (C_1, ^1A)	−0.21862/−0.10945	2.97	7.08	1.84
NiP(β-CF_3)$_8$ (C_1, ^1A)	−0.24566/−0.13839	2.92	7.94	2.55
NiP(β-NO_2)$_8$ (C_1, ^1A)	−0.28301/−0.18542	2.66	8.90	3.87
NiP(P)$_4$	−0.19496/−0.10062	2.57	6.51	1.46